京都大学防災研究所年報 第 49 号 C 平成 18 年 4 月

Annuals of Disas. Prev. Res. Inst., Kyoto Univ., No. 49 C, 2006

Research Works for the Risk Assessment Technology of Flood in Urban Area and Its Practical Application

Tomotsuka TAKAYAMA, Kaoru TAKARA, Keiich TODA, Masaharu FUJITA
Hajime MASE, Yasuto TACHIKAWA, Nozomu YONEYAMA,
Daizo TSUTSUMI and Tomohiro YASUDA

Synopsis

The present paper describes tentative results which have been obtained from the following research topics in our COE project on Risk Assessment Technology of Flood in Urban Area and Its Practical Application: 1) Methodological development for assessing habitat condition associated with bed variation, 2) Flood control by appropriate dam operation, 3) Prediction model for inundation of underground spaces, and 4) Experimental investigation on tsunami transformation due to a cross-shore shape of a sea bottom.

Keywords: Simulation river bed change, Reservoir sedimentation, River flood control, Hydrological prediction system, Yodo River basin, Inundation in underground space, Numerical model of underground inundation, Tsunami deformation, Dispersion of solitons, Tsunami force

1. Introduction

The research on the risk assessment technology of flood in urban area and its practical application has been performed by the Fluvial and Coastal Research Division as a part of the 21st Century COE Research Project. This paper briefly describes the results of the research activities performed by the Division in the Japanese fiscal year of 2005. The research activities in the paper are classified into four research topics: 1) Methodological development for assessing habitat condition associated with bed variation, 2) Flood control by appropriate dam operation, 3) Prediction model for inundation of underground spaces, and 4) Experimental investigation on tsunami transformation due to a cross-shore shape of a sea bottom.

2. A method for assessing habitat condition associated with bed variation

2.1 Change of void structure of bed material

Installation of dams on a river typically blocks the downstream delivery of sediment and causes the bed degradation and the river morphological change. Also, after the dam construction, the riverbed changes qualitatively, and consequently it is covered by an armor coat composed of coarser sediment and with a large porosity. For such reservoir sedimentation issues, recently sediment flashing has been implemented. Such an artificial sediment supply must influence the downstream reach quantitatively and qualitatively. From an ecological point of view, those human impacts on habitat for fish and aquatic insects are very important and particularly the importance of assessing the change in void structure of the bed material has been pointed out strongly.

A numerical simulation method for bed variation is one of the most powerful tools for assessing the influence of dam construction and sediment flushing. Some bed variation models are available to the numerical analysis on topographical and morphological changes of rivers. However, they are not useful for assessing the change in void structure at all because they are not equipped with a routine for the void structural change.

So far, we have conventionally assumed that the porosity of bed material is a constant in their bed variation models, regardless of whether the particle size of the bed material is uniform. However, if only fine sands are removed from a riverbed composed of sediment mixture or they deposit into the voids of coarser bed material, the porosity of the bed material must change significantly. For these situations, it is very clear that fixing the porosity at a constant value is inadequate in calculating the bed variation. Hirano (1971) has presented a bed variation model for sediment mixture, but also pointed out this necessity

of considering the change of porosity in some cases. After his activity, many researchers have developed a lot of numerical bed variation models, but nobody has proposed a model available for the analysis of change of porosity.

This study aims at developing a fundamental framework of qualitative and quantitative bed variation models to simulate the change both of void structure and bed variation. Firstly, a packing model of spherical particle was developed to analyze the void structure of sediment mixtures. Simulation was conducted to elucidate a relation between the porosity of sediment mixture with a grain size distribution and the standard deviation. Secondly, relating the porosity to the grain size distribution of sediment mixtures and installing the relation into a standard one dimensional bed variation model, we have built up a framework of advanced bed variation models able to assess changes of porosity. A simplified multi-layer model was introduced to obtain time and space variations of porosity of bed material. Then, a primitive model applicable for a mixture of two particle groups with much different grain sizes is presented in this framework. Finally the model was applied to the simulation of reservoir sedimentation.

2.2 A particle packing model

A model putting a set of particles into a hypothetical vessel was made and it was used to obtain the porosity of sediment mixtures. The size of a packed particle and the packing order are determined from the grain size distribution using random number. The particle is put on as low a position as possible in the vessel. Porosity of a sediment mixture depends on not only the grain size distributions but also the compaction. The compaction, however, can not be intentionally controlled in the model. As a result of packing simulation, the compaction degree is given. The packing rules are as follows (Fig.2.1):

(i) 1st particle is put on the origin of the coordinate axes.
(ii) 2nd particle is put on the *x*-axis so that the particle contacts the first particle.
(iii) 3rd particle is put on the *x*-*y* plane so that the particle contacts the first and second particles.
(iv) *n*-th particle is put on as low a position as possible where it contacts three other fixed particles, or on any available position on the *x*-*y* plane where it contacts two other fixed particles.
(v) If *n*-th particle is placed $d_{max}/2$ away from the side walls or bottom plane of the vessel, that point is excluded, where d_{max} is a diameter of the largest particle.
(vi) If *n*-th particle is placed $d_{max}/2$ away from top of the vessel, the packing simulation terminates.

To assess the validity of the packing model, a laboratory experiment was conducted. Spherical glass beads with 6 different diameters (i.e., 0.2, 0.4, 0.6, 0.8, 1.0, and 2.0mm) were mixed well to form 6 different grain size distributions. The glass bead mixture was put into a cylindrical vessel and the porosity was obtained. This procedure was repeated 5 times and 5 data on the porosity were taken for each mixture. Simulation of the experiment was carried out five times for each mixture. The simulated average porosity of each material agrees with the experimental one as shown in Fig.2.2. However, concerning the deviation, some problems are remained in the model. Firstly, the simulated porosity of a uniform material (No.1) ranged widely from 0.280 to 0.351. The lowest value agrees with the theoretical value of the densest packing, but the mean value differed from it. This result shows that this simulation procedure does not always create the situation of the densest packing and produces a different packing situation even for the uniform material. Secondly, the deviation of the simulation result is much higher than the experiment result. The material selected with random number has a somewhat different particle size distribution from the actual one. This is a reason why the deviation of the simulation result does not agree with the experiment result. There are some problems to be modified, but the presented packing model is applicable to estimating the porosity of sediment mixtures.

2.3 Porosity of sediment mixtures

Armor coats have usually Talbot type of grain size distribution, but riverbed materials have often the lognormal distribution. Thus, we discuss the porosity of sediment mixtures with lognormal grain size distributions. Porosity of the material with a standard deviation of 0 to 1.5 was calculated by means of the packing model. A relationship between the standard deviation, $\ln\sigma$, and the calculated porosity is shown in Fig.2.3. If the standard deviation $\ln\sigma$ is between 0.01 and 0.1, the porosity is about 0.38. This value is close to the value (0.4) generally used in conventional calculations on riverbed variation. The porosity decreases to 0.156 when the

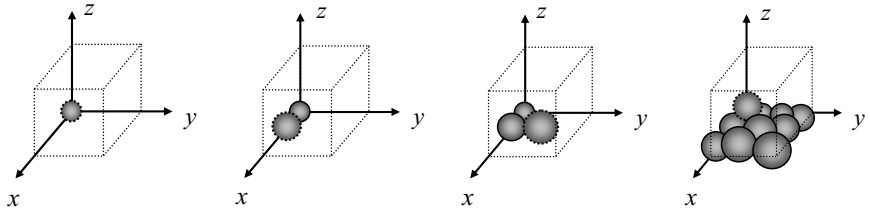

Fig.2.1 How to put particles selected with random number into a hypothetical vessel

standard deviation lnσ increases to 1.50. When the particle size is widely distributed, the porosity takes much smaller value than 0.4. The porosity measured on a sandbar was reported to be 0.16 (Takemon et al., 2003). This supports our simulation result. Another interesting result is found in Fig.2.3. The porosity increased to 0.38 when the standard deviation lnσ increase slightly from 0. This means that the porosity increases drastically if particles with a different size are put into a uniform material.

2.4 Voids within the packed particles

We can visualize the void structure by cutting a hypothetical vessel filled with a sediment mixture. Fig.2.4 shows four cross-sections in the case of sediment mixture of lognormal distribution with a standard deviation of 0.5. The particles are more densely packed at the lower position. From this figure, the spaces among particles are obtained quantitatively and such a result could give important information to a habitat condition for the aquatic living things.

2.5 Coupling bed variation model and packing model

(1) General concept

Porosity of bed material is associated with the grain size distribution using the presented packing model. The change of grain size distributions is calculated by means of the previous bed variation models. If these models are coupled, the change in void structure is analyzed with bed variation. As the packing simulation, however, takes too much time to obtained a result, the linkage is impossibly difficult. The simulation result on a relation between porosity and grain size distribution is, therefore, introduced into a bed variation model.

(2) Basic equations

Basic equations are the same as those employed in general previous bed variation models. In this section, equations different from them are explained below. A continuity equation of sediment shown in Eq.(2.1) is usually employed for a one-dimensional numerical simulation of bed variation. For a sediment mixture, Eq.(2.2) or (2.3) that is proposed by Hirano (1971) are coupled to Eq.(2.1) to calculate the change of grain size distribution of bed material.

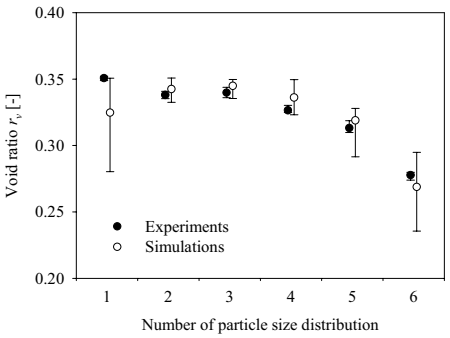

Fig.2.2 Comparison between the experiment result and the simulation result on porosity

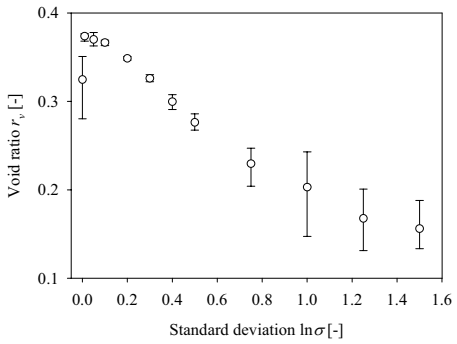

Fig.2.3 The relation between the porosity and the standard deviation of sediment mixture

$$\frac{\partial z}{\partial t}+\frac{1}{(1-\lambda)B_s}\frac{\partial Q_B}{\partial x}=0 \tag{2.1}$$

$$\frac{\partial f_j}{\partial t}=\frac{-1}{(1-\lambda)aB_s}\frac{\partial Q_{Bj}}{\partial x}-\frac{f_j}{a}\frac{\partial z}{\partial t} \qquad \left(\frac{\partial z}{\partial t}\geq 0\right) \tag{2.2}$$

$$\frac{\partial f_j}{\partial t}=\frac{-1}{(1-\lambda)aB_s}\frac{\partial Q_{Bj}}{\partial x}-\frac{f_{j0}}{a}\frac{\partial z}{\partial t} \qquad \left(\frac{\partial z}{\partial t}<0\right) \tag{2.3}$$

where t = time, x = flow direction, z = bed elevation, λ= porosity of bed material, B_s = channel width, Q_B = sediment discharge, f_j = proportion of grain size d_i in surface bed material, f_{jo} = proportion of grain size d_j in subsurface bed material, Q_{Bj} = sediment discharge of d_j and a = thickness of exchange layer of bed material and transported sediment.

It is recognized that numerical simulation using these equations could create a reliable result on bed variation. This model, however, can not explain the

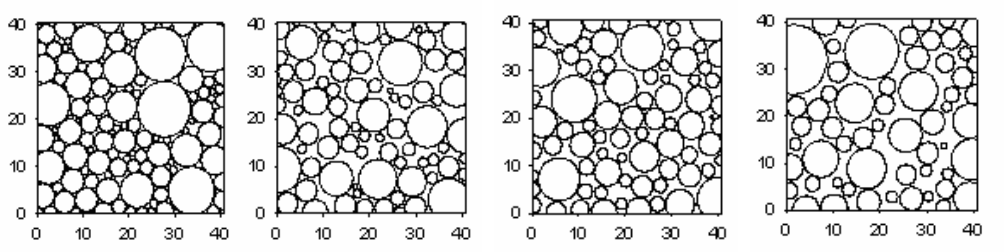

Fig.2.4 Cross section of a vessel filled with a sediment mixture whose size distribution is lognormal distribution with a standard deviation of 0.5

change in void structure with bed variation because it assumes that porosity is always constant. The model, therefore, can not be applied to the condition under which the porosity is changed. From an ecological point of view, we need to analyze such a qualitative change. For such a analysis, we have to consider the change of porosity and employ Eq.(2.4) instead of Eq.(2.1).

$$\frac{\partial}{\partial t}\left\{\int_0^z (1-\lambda)dz\right\}+\frac{1}{B}\frac{\partial Q_B}{\partial x}=0 \qquad (2.4)$$

Porosity of sediment mixture is dependent only on the grain size distribution in our model. Eq.(2.4) is, therefore, solved with Eq.(2.2) and (2.3). Thus, bed variation is calculated using Eq.(2.2), (2.3) and (2.4), but a numerical simulation method for such implicit differential equations is required.

(3) A Layer model of riverbed

The space distribution of porosity of bed material and its time variation are necessary to solve Eq.(2.4). To obtain them, it is convenient to build up a layer structure in riverbed. Each layer is numbered from the surface layer (i.e. 1st layer is surface layer). The thickness of each layer is assumed to be equal to the maximum size of bed material. We assume that the exchange between bed material and transported sediment take place within the surface layer and sediment transportation from an upper layer to the lower layer is neglected. These assumptions are contradicted with a fact that finer sediment possibly drops into the lower layer of gravel-cobble bed. For convenience' sake, however, those conditions are excluded in this model.

The equations are solved by means of a finite differential method. So, the calculation grid structure whose lateral and vertical intervals are Δx and a respectively is made in riverbed. Considering the mass balance of sediment, the increase in bed elevation Δz during time Δt is expressed by the following equation.

$$\Delta z=\frac{1}{1-\lambda_2^t}\left\{\left(\lambda_1^{t+\Delta t}-\lambda_1^t\right)a-\frac{\Delta t}{B\Delta x}\left(Q_{Bi}^t-Q_{Bi-1}^t\right)\right\} \qquad (\Delta z<0) \quad (2.5)$$

$$\Delta z=\frac{1}{1-\lambda_2^{t+\Delta t}}\left\{\left(\lambda_1^{t+\Delta t}-\lambda_1^t\right)a-\frac{\Delta t}{B\Delta x}\left(Q_{Bi}^t-Q_{Bi-1}^t\right)\right\} \qquad (\Delta z>0) \quad (2.6)$$

where λ_n^t= porosity of n-th layer at time t, Δx = space interval in flow direction and Q_{Bi}^t = sediment discharge at time t and section i.

$\lambda_1^{t+\Delta t}$ and $\lambda_2^{t+\Delta t}$ necessary for calculate Eq.(2.5) and (2.6) are associated with the grain size distribution of 1st and 2nd layers at time $t+\Delta t$. As mentioned before, Eq.(2.2), (2.3) and (2.4) are a set of implicit differential equations. To simplify the numerical method, the grain size distribution of 1st layer at time $t+\Delta t$ is calculated by Eq.(2.7).

$$f_{j,1}^{t+\Delta t}=\frac{f_{j,1}^t\left(1-\lambda_1^t\right)a\Delta x+\Delta t\left(Q_{Bi,j}^t-Q_{Bi-1,j}^t\right)r_B}{\left(1-\lambda_1^t\right)a\Delta t+\Delta t\left(Q_{Bi}^t-Q_{Bi-1}^t\right)r_B} \qquad (2.7)$$

where $r_B=\frac{1}{2}\left(B_i+B_{i-1}\right)/B_i$.

The grain size distribution of 2nd layer at time $t+\Delta t$ is also assumed to be equal to $f_{j,1}^{t+\Delta t}$.

(4) Application

The presented bed variation model is applied to a problem on the bed variation in the upstream of a weir. The channel length and the initial slope are 2,000 meters and 0.01, respectively. The unit water discharge is 2.5m^2/s. The water depth at the weir section is 5m. Simulation was conducted for two cases. In case 1, a fine sand of 0.1 cm is supplied to a riverbed covered by an armor coat. The armor coat is composed of a gravel of 20cm. In the case 2, no sediment is supplied, but the bed material is composed of the sand and the gravel. Simulation on the bed variation and the change in voids was carried out for the material composed of 2 particles.

As the previous bed variation model, sedimentation process was simulated. In this condition, the bed level at the sections far from the weir does not change because the gravel does not move. The previous method where the change in porosity is not considered creates the deposition or erosion, but the presented method can simulate the bed variation reasonably. Fig.2.5 shows the vertical distribution of porosity of bed material. In case 1 the porosity of the first layer at x=500m decreases from the initial value because the supplied sediment come into the layer, and in the case 2 it increases because the fine sand in the bed material is removed. In the case 1, the vertical distribution of the porosity of the sedimentation near the weir is calculated adequately.

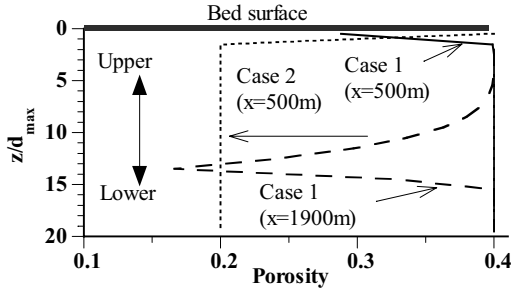

Fig.2.5 Simulation result on vertical distribution of porosity

3. Flood control by appropriate dam operation

3.1 Introduction

The alterations of hydrological cycle caused by environmental change indicate that observed information with past or current conditions may not be applicable for future predictions. It is essential for risk assessment of flood to understand the scientific background of hydrological alterations induced by human activity and to predict the future hydrological cycle based on the understandings. One of the crucial flow regime changes is caused by dam reservoirs.

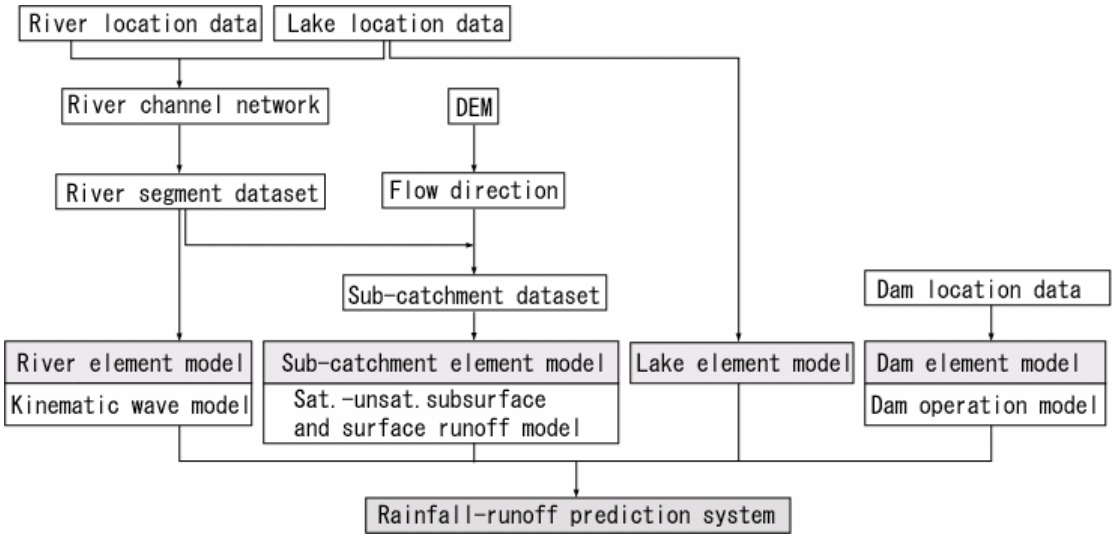

Fig.3.1 Data processes and the whole structure of the system

There are mainly two approaches for the assessment of flow regime change induced by dam reservoirs. One is the data driven approach, which uses discharge data observed before and after dam constructions; the other one is model approach, which uses hydrological models incorporated with dam reservoir models. The advantage of the model approach is the possibility of conducting various hypothetical experiments such as simulating inexperienced extreme flood events.

We focus on flood control with multi-purpose dams, which are operated in a complicated manner based on dam operation rules. The developed dam model in this study predicts outflow and water level with the input information of inflow, upstream rainfall and cooperative dam operations by modeling dam operation rules. A hydrological prediction system is constructed by incorporating the dam models with a distributed rainfall–runoff model. We developed this system for a highly regulated Japanese river basin, the Yodo River basin (7281 km^2). By using the developed system, we assess dam effects on flood control to investigate how the flood safety level has been increased by newly constructed dams and to understand which range of flood magnitudes the dams can regulate effectively.

3.2 A distributed rainfall–runoff prediction system incorporating dam operation model (Sayama, 2005)

(1) Structure of the rainfall–runoff prediction system

The rainfall–runoff prediction system is constructed based on "Object-oriented Hydrological Modeling System (OHyMoS)". The following four kinds of element models compose the whole system (Fig.3. 1).

(a) River element model: The kinematic wave model is applied to a river segment, which is prepared from the digital river-network data and the location information of lakeshores. Each river segment is cut to be about 3 km length.

(b) Sub-catchment element model: A saturated - unsaturated subsurface and surface runoff model (Tachikawa et al. 2004) is applied to all grid-cells composing a sub-catchment. We used a digital elevation model with 250 m resolution to calculate the flow direction and to define the sub-catchment of each river segment.

(c) Lake element model: Lake element model is a simple mass-balance model to simulate water level from inflow, outflow, and rainfall information. We apply this model to Lake Biwa, of which outflow is simulated with the dam element model.

(d) Dam element model: A dam operation model is constructed with if-then style based on each dam operation rule. We apply it to eight multi purpose dams in the basin. We refer this site-specific dam operation model as a dam element model.

(2) Dam element model

By formulating the dam operation rules and decision-making processes of dam operators, we develop the dam operation model. It predicts the outflow and water level of a dam with the input information of inflow, average rainfall in the dam catchment, and operation status of other related dams.

All the dams located in the Yodo River basin are multi-purpose dams. Although each dam has different operating rules, we can categorize all the flood control operations into the following six common operation processes (Ichikawa, 2001): Ordinary operation; Operation under flood warning; Preliminary release operation; Peak attenuation operation; Flood release operation; and Post flood operation.

Each dam is always under one of the six operations, and we formulate the conditions to shift from one operation to another with if-then equations. Fig.3.2 (left) shows how to shift the process from one to another, and Fig.3.2 (right) shows specific water levels that appear in the dam operation rules.

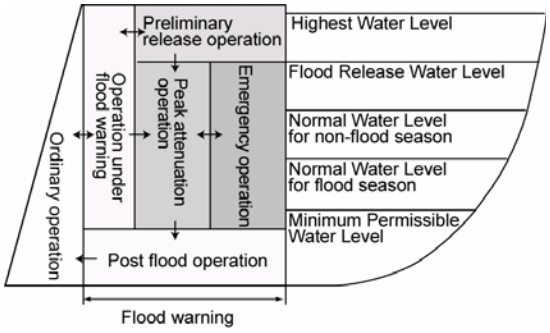

Fig.3.2 Operation statuses and specific water levels of dam operation model

3.3 Application to the Yodo River Basin

(1) Study area

The Yodo River basin is analyzed in this case study because it is a typical Japanese river basin highly regulated by multi-purpose dams. The total area of the Yodo River basin is 8240 km^2. In this case study, since Hirakata is the main design target location for designing dams and other river works, we focus on the upper Hirakata basin (7281 km^2) (Fig. 3.3), and refer to this basin as the Yodo River basin in this paper.

There are eight multi-purpose dams inside the basin and five of these dams are located in one of the sub-basins, called the Kizu River basin (1596 km^2). The Setagawa weir controls outflow from Lake Biwa (670 km^2), which is the largest Lake in Japan. The mean annual precipitation of the Yodo River basin is about 1600 mm.

We conducted a test simulation using observed rainfall and observed discharge data during a typhoon event in 1997. The period of the simulation is from 25 July to 29 July. We used the nearest neighbourhood method to distribute rainfall data that is observed by 58 raingauge stations inside the basin. The estimated total rainfall over the basin is 149 mm.

We divide the whole basin into three zones depending on the land use, and assign different parameters in the different land use zones. There are three land use categories: forest, paddy field, and urban area, among which forest is the dominant land-use (63%). A rainfall–runoff model considering surface flow is used for the paddy field zone and the urban area zone. Six dams and Biwa Lake are also simulated in the rainfall–runoff simulation system. Two dams constructed after 1997 are not included in this simulation.

(2) Simulation results

Figure 3.4 shows the simulated and observed inflow and outflow at the Shorenji dam. The good agreement between the simulated inflow with the observed inflow verifies the rainfall–runoff model at the upstream of the dam. The outflow from the dam operation model shows that the preliminary release and peak attenuation operations were properly simulated. Figure 3.5 shows the simulated and observed water level at the Shorenji dam. It shows that the water level is drawn down by the preliminary release and it is increased by the peak attenuation operation.

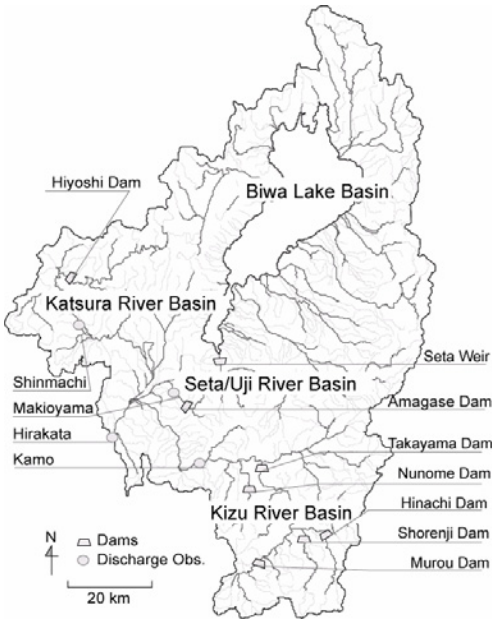

Fig.3.3 Yodo River basin (7281 km^2)

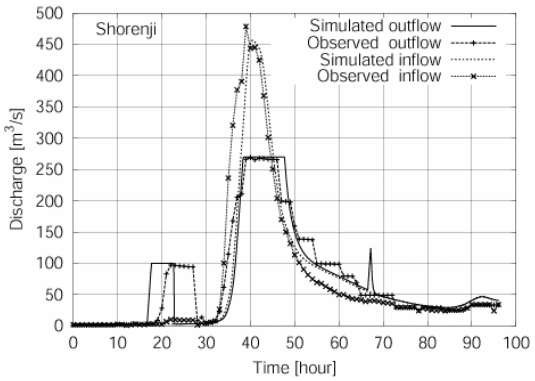

Fig.3.4 Simulated and observed inflow and outflow at Shorenji dam

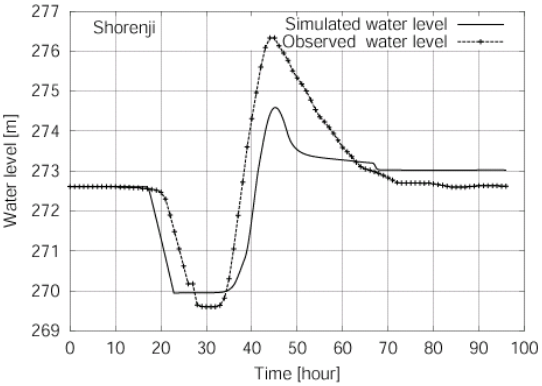

Fig.3.5 Simulated and observed water level at Shorenji dam

Figure 3.6 shows the simulated and observed discharge at Kamo. The simulation result excluding the dam element models is also displayed in the figure. By comparing simulated hydrographs with and without dams, it was concluded that the dams located upstream of Kamo could attenuate the peak flood by around 1300 m^3/s.

3.4 Analysis of dam effects on flood control

Construction of large-scale dams is believed to have improved the safety level of a catchment against flood disasters. However, it is not clear to what extent these dams have improved the safety level or which range of flood magnitudes dams can regulate efficiently. In terms of the Yodo River basin, there are currently eight large-scale dams in the basin and seven dams were constructed after 1960. Conducting rainfall–runoff simulation using the developed rainfall–runoff prediction system, we evaluate how the flood safety level of the Yodo River basin has been progressively increased over the period 1960 to 2000 with respect to rainfall events of different magnitude.

(1) Methods

Rainfall–runoff simulations were implemented considering the dams that were operated at the beginning of the following years: 1960, 1970, 1980, 1990, and 2000. The simulated peak discharges at Hirakata are examined to discuss the effect of the dams. The rainfall event used in this study is the typhoon event observed in 1982 (1–3 August). This event was chosen because it was the largest event since 1980 when enough rainfall–discharge sequences were available to conduct the simulation.

Furthermore, in order to examine which flood magnitude the dams can attenuate the peak, some factors were multiplied to the 1982 rainfall pattern. The factors are selected so that two-day total rainfall amounts in the Yodo River basin correspond to the following return periods: 30, 50, 100, 150, 200 and 300 years. The same parameters and the initial conditions used in the test simulation are used for this assessment.

(2) Results and discussion

Figure 3.7 shows the simulated peak discharge at Hirakata. The different lines represent different years. Firstly, looking at the results of 1960 when only the Setagawa weir existed, it can be observed that peak discharge caused by the 30-year return period rainfall (Q30) exceeds 12,000m^3/s, which is the allowable maximum flood discharge at Hirakata. By 1970 two other dams, the Amagase dam and the Takayama dam, had been constructed. The comparison between the lines for 1960 and 1970 indicates these two newly constructed dams successfully decrease flood peaks from relatively smaller rainfall events up to around the 50-year return period. By 1980, two more dams, the Shorenji dam and the Murou dam, had been constructed. These dams enabled the peak discharge to reduce by about 2000 m^3/s compared

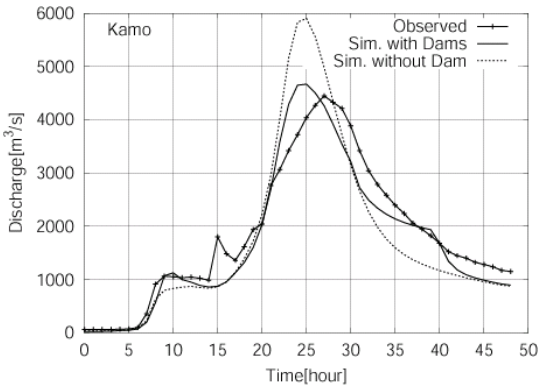

Fig.3.6 Simulated discharge (with and without dams) and observed discharge at Kamo

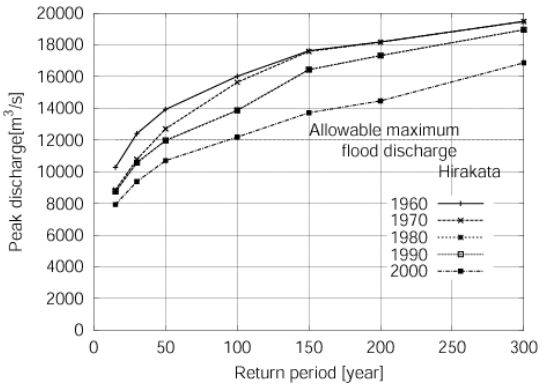

Fig.3.7 Simulated peak discharges at Hirakata with different magnitude of input rainfall. Years (1960, 1970, etc.) denote that the dams existed in the year are included in the simulation.at Kamo

with the discharge from the 100-year and 150-year return period rainfall. This is because the Takayama dam located at the downstream of the Shorenji dam and the Murou dam had a flood control capacity large enough to regulate floods of this magnitude. By 2000, a further three dams, the Nunome dam, the Hinachi dam, and the Hiyoshi dam, had been constructed. It is noteworthy that, in 2000, the allowable maximum flood discharge was exceeded by the discharge from the 100 year return period rainfall (Q100), whereas in 1960 this value was exceeded by the Q30 peak discharge.

4. Prediction model for inundation of underground spaces

4.1 Introduction

When flood flow hits the central district of large cities, the inundation flow would extend to underground space and the damage would be serious. In fact, urban floods such as the ones that occurred in Fukuoka, Japan in 1999 and in 2003 and the one that occurred in Seoul, Korea in 2001 induced inundation into underground space and caused extensive damage. Therefore, it is very significant to study the inundation in underground space from the hydraulic

and disaster preventive aspects.

Takahashi et al. (1990) first made an inundation flow model in underground space. They treated the inflow from stairs into underground space as a stepped flow. They also showed that a horizontally two-dimensional inundation flow model can be applied to underground space. In their studies, only simple underground shapes were treated, and the effect of ceiling in underground space was not taken into account. Toda et al. (2000) developed the underground inundation model based on the one-dimensional network model with a slot, and applied it to Umeda underground mall in Osaka, Japan. They could succeed in treating the real complicated underground space and expressing both of the open channel flow condition and the pressurized flow condition. In their model, however, the flow behavior cannot be well simulated under some conditions of roughness coefficient, inflow discharge and slot area. In addition, many problems arose for acquisition and reduction of underground geographical data.

In view of these situations, a solid numerical simulation model named the storage pond model is developed for underground inundation based on a pond model (Toda et al., 2004). This model is simper than the above stated models. The data required for the model is reduced. Also, this model can treat both ground and underground inundation simultaneously without much difficulty. In this paper, the storage pond model is applied to the central area with underground spaces in two large cities in Japan, Fukuoka City and Kyoto City, and the inundation flow behaviors in both ground and underground are studied in detail.

4.2 Simulation method

Underground spaces such as shopping mall are generally composed of stores, open spaces, subway entrances and basements of adjacent buildings. Though the total underground mall may be very complicated, it can be divided into some parts. If each part is assumed to be a storage pond that has its own volume, the underground space is expressed by the combination of storage ponds in the three dimensions (see Fig.4.1).

The slot is also incorporated in each pond taking into account the pressurized flow condition. Thus, the dispersion of inundation water can be expressed by obtaining the discharge flowing between the adjacent storage ponds. For the inundation on the ground surface, the similar method can be applied, without slot in each pond.

The governing equations are the continuity equation and the momentum equation expressed below as follows:

(Continuity equation)

$$A\frac{dH}{dt} = \sum Q_i + Q_{ins} \qquad (4.1)$$

$$A = A_f : h < D, \quad A = A_s : h \geq D$$

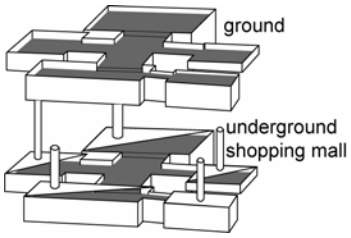

Fig.4.1 Storage pond model

where A is the effective base area of storage pond, H is water stage, Q_i is inflow discharge from i-th adjacent storage pond and Q_{ins} is lateral inflow discharge from the ground surface. H is water depth and D is the ceiling height of the storage pond. A_f is the area related to the storage pond shape and A_s is the slot area.

(Momentum equation)

$$\frac{L}{gA_b}\frac{dQ}{dt} = \Delta H - \alpha LQ|Q| \qquad (4.2)$$

where Q is discharge, g is gravity acceleration, and L is the distance between the base area centroids of adjacent storage ponds. A_b is the cross-sectional area of adjacent storage ponds, and it is determined according to the water depths in the adjacent storage ponds. ΔH is the water level difference between the adjacent storage ponds and α is loss coefficient associated with Manning coefficient.

At the inflow position from the ground surface to the underground space and the dropping position from the upper floor to the lower floor in multistory underground space, the following step flow formula is applied.

$$Q = B_e \mu_0 h_e \sqrt{g h_e} \qquad (4.3)$$

where, B_e is effective width of entrance, μ_0 is discharge coefficient and h_e is the water depth in the upper storage pond. If the lower storage pond is pressurized, then the above momentum equation is applied.

4.3 Application to Fukuoka City

(1) Studied area and computational conditions

Figure 4.2 shows the studied ground area of about 2.8km^2 and Fig. 4.3 shows the ground elevation distribution. The ground elevation becomes lower from the Mikasa River to the direction of JR Hakata station. Figure 4.4 shows the underground space under JR Hakata station. The subway track space is assumed a storage pond with large volume. The total area and volume of underground space except subway railroad space are about 5.2×10^4 m^2 and 16.9×10^4m^3 respectively.

As for the boundary condition, the overflow discharge from the Mikasa River obtained by Hashimoto et al. (2003) is imposed. Figure 4.5 shows the discharge hydrograph and Fig.4.6 shows the storage ponds to which the overflow discharge is allocated as the lateral inflow. The computation start

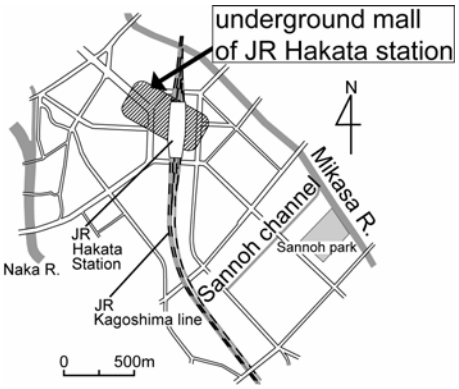

Fig.4.2 Studied area of Fukuoka City

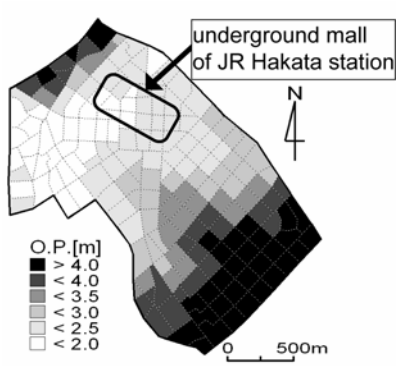

Fig.4.3 Fukuoka City ground elevation

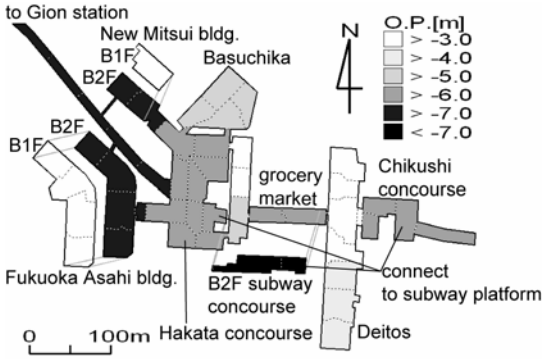

Fig.4.4 Studied area of JR Hakata station underground mall

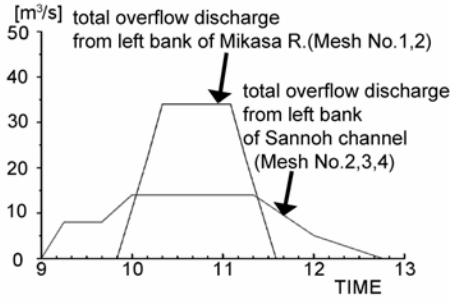

Fig.4.5 Inflow discharge hydrographs

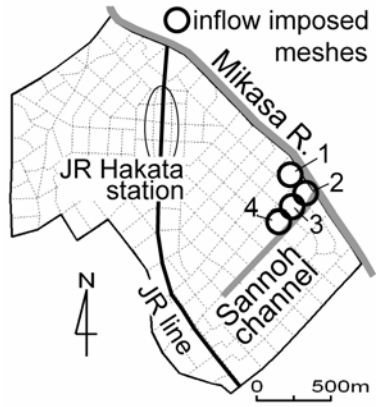

Fig.4.6 Inflow imposed meshes

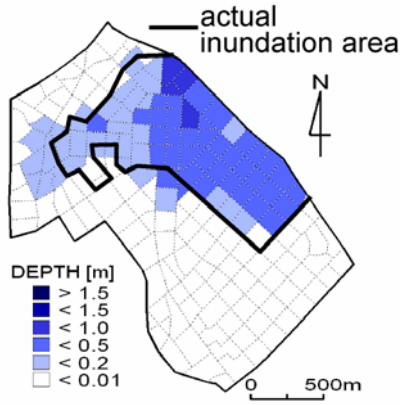

Fig.4.7 Maximum inundation depth on the ground

time is 9:00 on 29 June 1999 when the overflow began from Sannoh channel.

In the computation, the drainage by sewerage system of 36.4mm/hr, 70% of the designed value is considered. The inflow water into the basements of buildings and the water stored in the storage tank of the underground mall are also considered. Steps of entrance to underground space and pavement (30cm high in total) are also taken into account.

The values of Manning coefficient, n are 0.067 for ground and 0.03 for underground, respectively, and the discharge coefficient of drop formula is 0.544. The computational time step Δt is set to be 0.05s.

(2) Computational results

Figure 4.7 shows the comparison between the computed maximum water depth distribution and the actual inundation record on the ground. The computed inundated area shows good agreement with the actual inundation area. By this computation, the inflow water volume into the basements of buildings and the water volume stored in the storage tank of the underground mall amount to $6.0\times10^4 m^3$ and $1.3\times10^4 m^3$, respectively.

Figure 4.8 shows the computed maximum water depth distribution and the actual inundation record of the studied underground space. The computed result is in almost good agreement with the actual record. The computed water volume flowing into the subway track space is about $5000 m^3$ at 13:00, while the actual water volume is assumed $1000\text{-}2000 m^3$. This difference may be caused by the accuracy of

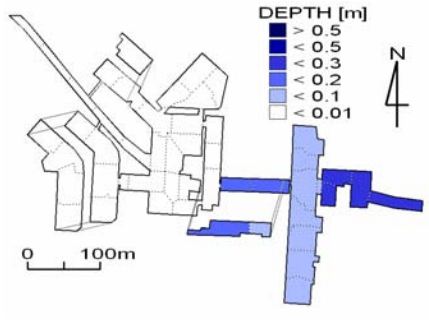

(a) Computation result

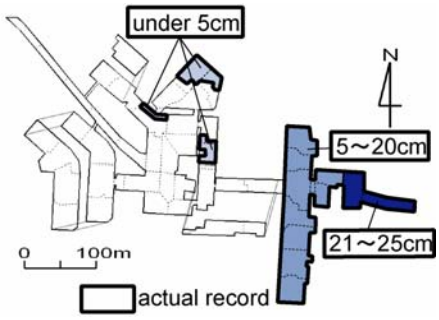

(b) Actual record at Fukuoka flood (1999)

Fig.4.8 Maximum inundation depth of the underground

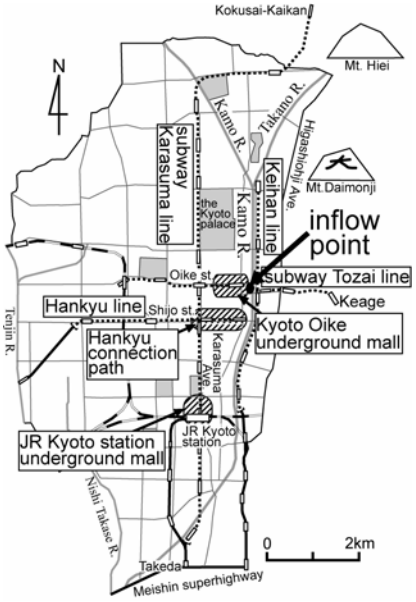

Fig.4.9 Studied area of Kyoto City

estimation of the water volume stored in the storage tank and the step height of the entrances to underground mall.

4.4 Application to Kyoto City

(1) Studied area and computational conditions

Figure 4.9 shows the studied area of Kyoto City of about 51.6km^2. The Kamo River runs in the central area. In the studied area, the underground spaces of Kyoto Oike underground mall, JR Kyoto station underground mall, the municipal subways and the railways privately operated are included. Figure 4.10 shows the structure of Kyoto Oike underground

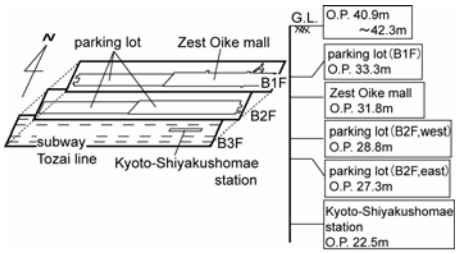

Fig.4.10(1) Kyoto Oike underground mall

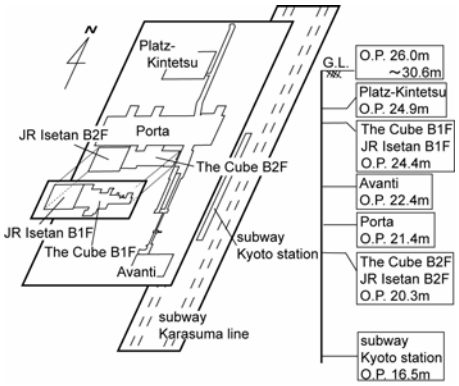

Fig.4.10(2) Kyoto station underground mall

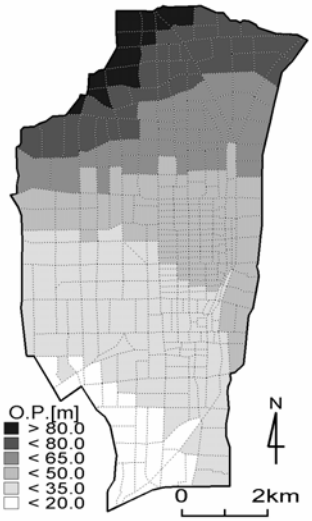

Fig.4.11 Kyoto City ground elevation

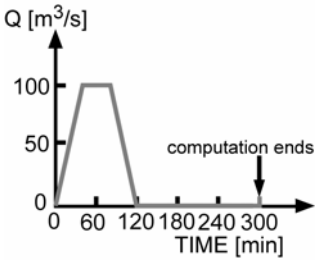

Fig.4.12 Inflow discharge hydrograph

mall and Kyoto station underground mall. Figure 4.11 shows the ground elevation distribution. Kyoto City is rather sloped from north to south.

In the computation, the river overflow in the central area is assumed and the hydrograph discharge shown in Fig.4.12 is imposed at the mesh along the

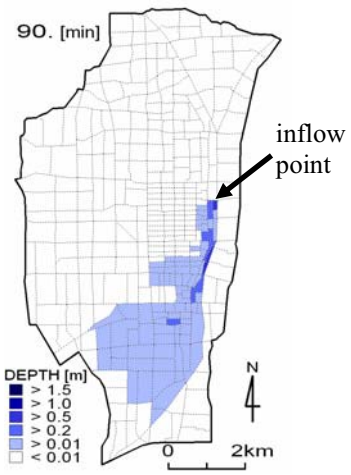

JR Kyoto station underground mall

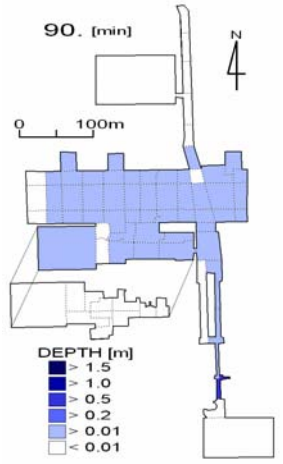

Kyoto Oike underground mall

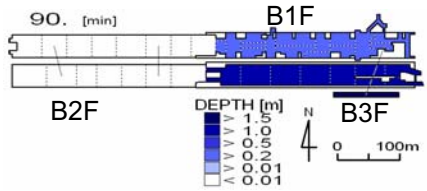

Subway Tozai line

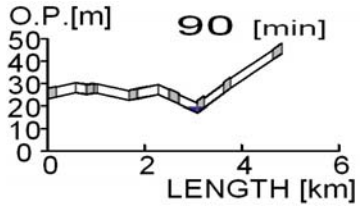

Fig.4.13 Computed inundation water depth distributions at 90min.

river as the lateral inflow. The parameter values used here are the same as those in the preceding section.

(2) Computational results

Figure 4.13 shows the computed inundation results of both ground and underground spaces at 90 min. after. The inundation water disperses from the overflow point to the south area, and it flows into Kyoto Oike underground mall, JR Kyoto station underground mall and subways. If the overflow occurs from this point, Kyoto Oike underground mall and the adjacent subway station are heavily submerged. In addition, the water flowing into the subway track space extends down to the next subway station. From this computational result, it is possible that the water flowing through subways inundates underground spaces that are far from inundation area of ground.

5. Experimental Investigation on tsunami transformation

5.1 Introduction

Japan has suffered from a large number of tsunami attacks since an ancient time. Many people were killed and valuable properties were lost due to the inundation of the tsunamis. A lot of memorial monuments have been constructed to memorize the past tsunami disasters for Japanese descendants and to secure their lives from attacks of tsunamis.

As well known, almost all tsunamis have been generated by submarine earthquakes with the seismic magnitude of more than seven (M>7), while very small number of tsunamis has been caused by volcanic eruptions and landslides. The disaster of tsunami which occurred off Shikoku was first recorded in 684. We can count the number of tsunami descriptions in Japan during past 1,400 years. The number reaches about 60 for 1,400 years. Six (6) disasters among 60 seems to have been caused by remote tsunamis which occurred in the sea very far from Japan. According to the count, the disastrous tsunamis occur once 20 to 30 years. Since the old descriptions are inaccurate, we selected believable and accurate documents recently described since the beginning of Meiji Era in 1968. Since Meiji, fifteen (15) disasters have taken place due to the tsunamis which occurred off Japan. This fact shows that a disastrous tsunami attacks Japan every about 10 years. If the disasters caused by the remote tsunamis are added to them, a disastrous tsunami occurs once seven years. Consequently, any part of Japan suffers from tsunami disaster every seven years on average.

The present paper describes transformation of tsunami. The tsunamis generated by submarine earthquakes are much transformed and amplified by spatial seabed topography and geography. Especially, tsunami force is much affected by its deformation which is closely related to the cross-shore shape. The deformation is characterized by the hydrodynamic experiments on tsunamis. It is also pointed out that the present hard and soft measures should consider tsunami behaviors in nearshore sea.

5.2 Deformation of tsunamis by the effect of cross-shore shape

The tsunami profile in the nearshore sea is much affected by the feature of cross-shore section and the power of the tsunami related to disasters depends on

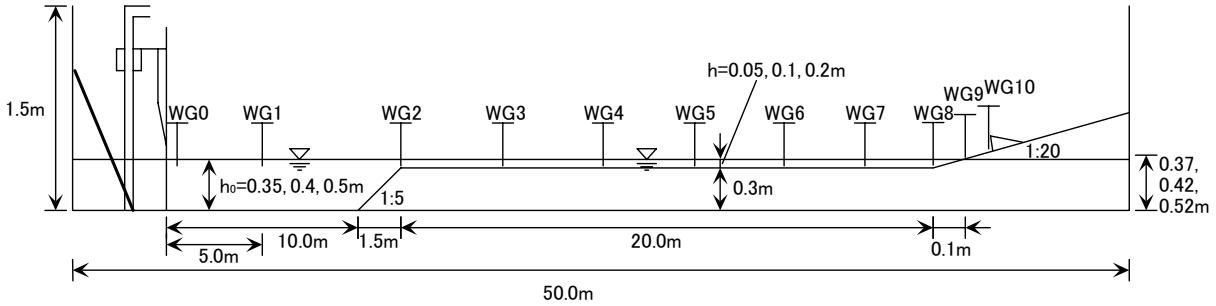

Fig.5.1 Experimental set-up

the profile of the tsunami. Present knowledge for the tsunami transformation due to the cross-shore shape can be mentioned as follows: When the slope of the cross-shore section is as gentle as less than 1/200, the front face of the tsunami becomes steeper and steeper during the propagation on the gentle slope, and short waves like normal wind waves appear near the crest of the tsunami (Tanimoto et. al., 1983). The appearance of the short waves is called soliton dispersion. Though the waves are small at their appearance, they develop gradually in their further propagation. The developed short waves break at a shallow sea near a shore and run-up on the shore. When the slope is comparatively steep, the tsunami is reflected from the shore and standing wave is formed by the superposition of the incident and reflected tsunamis.

Thus, the tsunami transformation is supposed to be related to the intensity of force on coastal structures. The hydraulic experiments were carried out to investigate characteristics of the tsunami transformation in more details.

(1) Experimental set-up

The cross-shore shape in the experiments is shown in Fig. 5.1. As shown in Fig. 5.1, flat reef of a uniform depth is connected with the shore of uniform slope of 1/20. The experiment employed the different water depths of 5cm (5m), 10cm (10m) and 20cm (20m), and a vertical barrier of 10cm (10m) high is placed on the shore at 2cm (2m) above the still water level to observe wave e pressure. The tsunami crest height and period in the experiments are 3cm (3m) and 30s (5min.). The figures in the parenthesis indicate the values in prototype as the model scale 1/100. The experimental results only for the water depths of 5cm and 10cm are discussed in this paper. Tsunami profiles are measured at 9 or 10 different points by capacitance type of wave gauge. They are indicated as WG. A model of a tsunami barrier was placed on the shore of 2cm above the still water level to measure tsunami pressures as shown in Fig.5.2. Three pressure meters is attached at different points of 1, 4 and 7cm above the shore surface.

(2) Case of water depth 5cm

The measured profiles of the tsunami at different 9 points are shown in Fig.5.3. The profile of the incident tsunami at WG1 is quite smooth in the deep water, and the tsunami crest height at WG2 increases to about 4cm from 3cm due to the shoaling effect

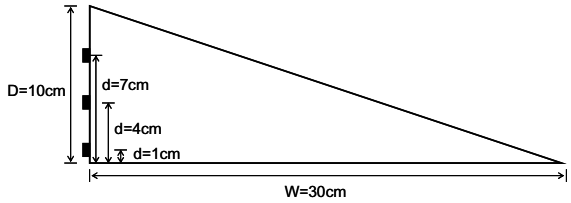

Fig.5.2 Model barrier and pressure measurement

because the tsunami climbs up on the shoulder of the shallow reef. The profile at WG3 which is 4m apart from WG2 shows that the soliton dispersion begins to take place on the front face of the tsunami after the tsunami propagates for the short distance of 4m on the shallow reef. The short waves created by the dispersion develop gradually, increasing their number as the measured profiles at WG4 show. The tsunami itself supplies energy to the short waves for their development and decreases its own crest height from 4cm to 3cm, as shown in the profiles at WG6 or 7. The short waves line up orderly from the higher to the lower. The highest first wave breaks first on the reef and decreased its height rapidly. The second wave becomes highest and breaks next. Thus the short waves break one after another and the group of the short waves loses its own energy. Almost all short waves break until the tsunami reaches the shore. Therefore the small waves after breaking remain as shown in the profile at WG10 just before the tsunami hits the barrier.

After the tsunami hits the barrier, it is reflected from the barrier and return toward offshore. The profiles at WG8 to WG5 clearly show the returning tsunami. The short waves continue to develop even on returning as far as sufficient water depth is secured by the effect of the incident tsunami. They begin to break when the water depth is low.

The profiles of the tsunami pressures measured at three different points on the barrier are shown in Fig.5.4. In the figure the black and grey lines respectively represent the pressures at 1cm and 4cm above the shore surface which is at 2cm above the still water level. The profiles of the observed pressures are quite similar to those of the tsunami at WG10 in Fig.10. The pressure measured at the point of 4cm implies that the water surface reached about 6cm above the measurement point, but the tsunami profile at WG10 does not reach there. The discrepancy is caused by difference of zero line

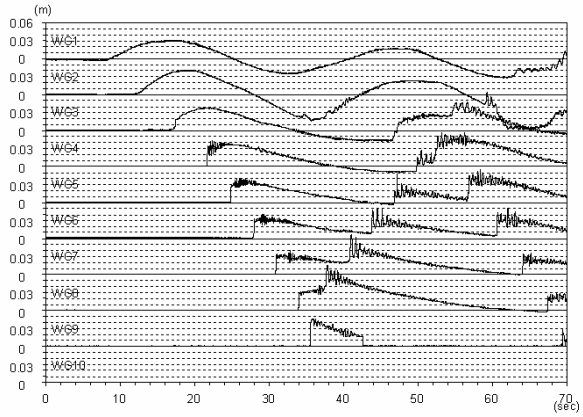

Fig.5.3 Tsunami profiles measured for water depth of 5cm

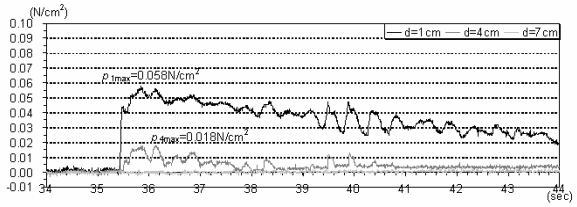

Fig.5.4 Pressure profiles for the water depth of 5cm

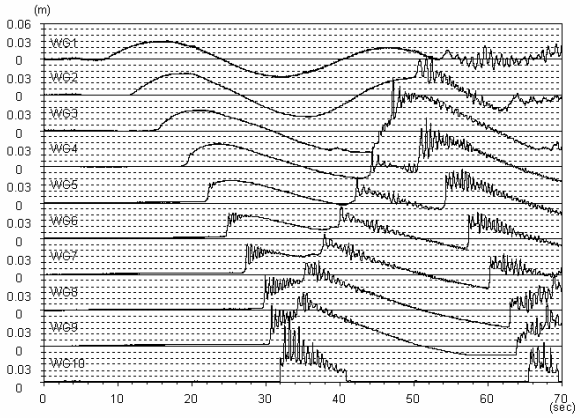

Fig.5.5 Tsunami profiles measured for water depth of 10cm

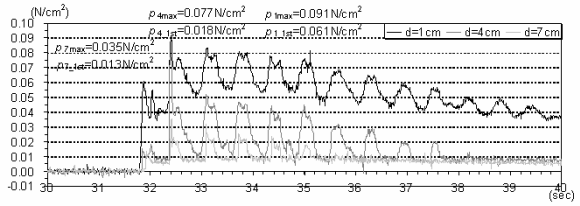

Fig.5.6 Pressure profiles for the water depth of 10cm

between the wave and pressure meters. The pressure profiles include small variations induced by the short waves after breaking, but their effect is small enough to neglect. The pressures correspond to static pressures induced by the tsunami itself.

(3) Case of water depth 10cm

The measured profiles of the tsunami are shown in Fig.5.5. The water depth above the reef becomes twice larger than that of the previous case. The incident tsunami of 3cm high at the crest is amplified to near 4cm by the effect of shoaling, but as the result of the increase of the water depth the amplification of the tsunami is slightly smaller than that of the previous case. The dispersion appears at WG4, and the short waves created by the dispersion grow larger as the tsunami propagates more. They develop even after the tsunami reaches the uniform slope of the shore. The highest first wave develops up to about 4cm high at WG8 of the toe of the uniform slope and breaks between WG9 and WG10. Just before the tsunami arrives at the barrier, the second wave begins to break and hits the barrier in the state of breaking. The tsunami returns toward offshore by the reflection from the barrier.

The profiles of the tsunami pressures measured at three different points are shown in Fig.5.6. In the figure the black, grey and light grey lines respectively represent the pressures at 1cm, 4cm and 7cm above the shore surface. The effect of the short waves on the tsunami pressures can be quite distinguished. The second wave in the state of breaking exerts large impulsive pressure on the barrier. Excluding the static pressure induced by the tsunami itself, the largest pressure appears at the point of 4cm above the shore. Including the static pressure, the largest pressure takes place at the lowest point of 1cm above. Though the incident wave height is same as that of the previous case, the maximum pressure is 1.5 times larger than that of the previous case. The excess pressure is caused by the influence of the short waves because the short waves are quite dynamic.

Though experimental results for the case of 20cm deep above the reef are not shown here, it can be added that the dispersion and the short waves are not distinguishable and the affection of the short waves on tsunami pressures is small enough to be negligible.

6. Concluding Remarks

The following main conclusions are drawn for four research topics:

(1) A method for assessing habitat condition associated with bed variation

1) A packing model of spherical particle was developed to analyze the void structure of sediment mixtures. Simulation was conducted to elucidate a relation between the porosity of sediment mixture with a grain size distribution and the standard deviation.
2) Relating the porosity to the grain size distribution of sediment mixtures and installing the relation into a standard one dimensional bed variation model, we have built up a framework of advanced bed variation models able to assess changes of porosity. A simplified multi-layer model was introduced to obtain time and space

variations of porosity of bed material. Then, a primitive model applicable for a mixture of two particle groups with much different grain sizes is presented in this framework.

3) The model was applied to the simulation of reservoir sedimentation.

(2) Flood control by appropriate dam operation

A rainfall–runoff prediction system was developed for the Yodo River basin. The combination of the dam operation models and the rainfall–runoff models enabled to simulate highly regulated rainfall–runoff processes. The conclusions of the assessment of dam effects on flood attenuation in the basin are summarized as follows:

1) The dams constructed in the 1960s were effective in attenuating relatively small flood peaks caused by the rainfall event with the magnitude of the 50-year return period or smaller. On the other hand, the dams constructed after 1970 were effective in attenuating relatively larger flood peaks caused by the rainfall events with the magnitude of the 100-year return period or larger.
2) Q30 corresponds to the allowable maximum Q30 corresponds to the allowable maximum flood discharge at Hirakata in 1960, while Q100 corresponds to it in 2000. However, we found that it has not achieved the initial design target: the discharge caused by smaller than the 200-year return period rainfall cannot exceed the allowable maximum flood discharge.

As it is discussed in this paper water cycle in a catchment and flood potential are altered by human activity, which makes observed historical records not applicable directly for future predictions. Modelling water cycle and the effect of human activity such as dam reservoir operations is one of the solutions for this type of ungauged basins.

(3) Prediction model for inundation of underground spaces

The simulation model is developed which can treat both of ground and underground water inundation in urban area. Through the application of this model, the risk of underground inundation by heavy rainfall or overflow from the river in a large city will be discussed in more practical way.

(4) Experimental investigation on tsunami transformation due to a cross-shore shape of a sea bottom

The cross-shore shape much deforms the profile of the tsunami and produces the short waves when some conditions of the cross-shore shape and the tsunami are satisfied. The short waves strongly affect the intensity of tsunami pressure on barriers. The cross-shore shape is very important for the design of effective barriers and for the description of helpful hazard map to refugees. Effect of the cross-shore shape on the tsunami deformation and force is a new and urgent problem to be solved.

References

Hashimoto, H., Park, K. and Watanabe, M. (2003): Overland flood flow around the JR Hakata-eki station from the Mikasa and Sanno-Channel River in Fukuoka City on June 29, 1999, Journal of Japan Society for Natural Disaster Science, JSNDS,Vol.21, No.4, pp.369-384. (in Japanese)

Hirano, M. (1971): River-bed degradation with armoring. J. JSCE., 195, pp.55-65. (in Japanese)

Ichikawa, Y. (2001): Framework and lumping of distributed rainfall–runoff models. Dr Eng. Thesis, Kyoto University, Kyoto, Japan (in Japanese).

Sayama, T., Tachikawa, Y., Takara, K. and Ichikawa, Y. (2005): Development of a distributed rainfall-runoff prediction system and assessment of the flood control ability of dams (in Japanese). J. of Hydr.,Costal and Env. Eng., JSCE, 803 / II-73, pp. 13-27.

Tachikawa, Y., Nagatani, G. and Takara, K. (2004): Development of stage-discharge relationship equation incorporating saturated-unsaturated flow mechanism (in Japanese). Ann. Hydraul. Eng, JSCE, 48, pp. 7-12.

Takahashi, T., Nakagawa, H. and Nomura, I. (1990): Simulation method on inundation in an underground space due to intrusion of overland flood flows, the Annuals of the Disaster Prevention Research Institute, Kyoto University, No.33, B-2, pp.427-442. (in Japanese)

Takemon, Y., Tanida, K., Nakajima, T. and Mitamura, O. (2003): Qualitative investigation of hyporheos by the freeze-core-method. Proc. of Fluvial Creature Research Workshop, pp.235-241. (in Japanese)

Tanimoto, K. et al. (1983): Field and laboratory investi-gation of the tsunami caused by 1983 Nihonkai Chubu Earthquake, Tech. Note of PHRI, No.470, 100p. (in Japanese)

Toda, K., Inoue, K., Maeda, O. and Tanino, T. (2000): Analysis of overland flood flow intrusion into underground space in urban area, Journal of Hydroscience and Hydraulic Engineeri0ng, JSCE, Vol.18, No.2, pp.43-54.

Toda, K., Kuriyama, K., Oyagi, R. and Inoue, K. (2004): Inundation analysis of complicated underground space, Journal of Hydroscience and Hydraulic Engineering, JSCE, Vol.22, No.2, pp.47-58.

都市水害の危険度評価技術とその社会的応用に関する研究

高山知司・寶　馨・戸田圭一・藤田正治・間瀬　肇・立川康人・米山　望・堤　大三・安田誠宏

要　旨

本報告は，21 世紀 COE プロジェクトの一研究課題である「都市水害の危険度評価技術とその社会的応用に関する研究」に係わる以下のような研究テーマに関して 2005 年に行った研究の成果を概述したものである．１）河床変動に伴う生態の生息条件評価手法の開発，２）適切なダム操作による洪水制御，３）地下空間の浸水予測モデル，４）岸沖方向の海底床形状による津波の変形に関する実験的研究.

キーワード：河床変動のシミュレーション，貯水池流砂，洪水制御，水文予測システム，淀川流域，地下空間の氾濫，地下浸水数値計算モデル，津波の変形，ソリトン分裂，津波力